PHYSICAL REVIEW D **96,** 015011 (2017)

Constraining new physics models with isotope shift spectroscopy

Claudia Frugiuele, Elina Fuchs, Gilad Perez, and Matthias Schlaffer

Department of Particle Physics and Astrophysics, Weizmann Institute of Science, Rehovot 7610001, Israel

(Received 14 May 2017; published 12 July 2017)

Isotope shifts of transition frequencies in atoms constrain generic long- and intermediate-range interactions. We focus on new physics scenarios that can be most strongly constrained by King linearity violation such as models with $B-L$ vector bosons, the Higgs portal, and chameleon models. With the anticipated precision, King linearity violation has the potential to set the strongest laboratory bounds on these models in some regions of parameter space. Furthermore, we show that this method can probe the couplings relevant for the protophobic interpretation of the recently reported Be anomaly. We extend the formalism to include an arbitrary number of transitions and isotope pairs and fit the new physics coupling to the currently available isotope shift measurements.

DOI: 10.1103/PhysRevD.96.015011

I. INTRODUCTION

The standard model (SM) of particle physics is one of the most successful scientific theories. Yet, it cannot be a complete description of nature because, for example, it does not provide a viable dark matter candidate and cannot account for the observed baryon asymmetry of the Universe. The energy scale associated with new physics (NP) is unknown and therefore the experimental program for physics beyond the SM should be as broad as possible. As colliders are one of the main tools to study elementary particles, the LHC is pushing forward the energy frontier. A complementary and vital role is played by low-energy, precision, and high-intensity experiments, which require a joint effort of the particle, atomic, and nuclear physics communities. The MeV-GeV scale is already efficiently probed by a variety of high-intensity experiments [1–10]. The existence of new sub-MeV degrees of freedom can instead be probed by both astrophysical observations and precision experiments. In this context, atomic physics observables play an important role. For example, atomic precision measurements can be used to constrain interactions beyond the SM (BSM), see e.g. Refs. [11,12]. In a broader context, atomic physics probes have been used to test the violation of fundamental laws such as parity (see e.g. Refs. [13–20]), Lorentz symmetry [21,22], and even the time variation of fundamental constants of nature [23,24].

A new proposal to constrain NP using isotope shift measurements was presented in Ref. [25]. In Ref. [26] this proposal was detailed and it was shown that it can constrain new light degrees of freedom mediating long- and intermediate-range spin-independent interactions between electrons and neutrons. These new interactions cause a frequency shift that is factorized to a high degree into a product of a function that solely depends on the electronic degrees of freedom and a function that depends on the nuclear physics ones. Within the validity of this factorization, a linear relation between isotope shifts of different transitions is obtained. This is known as King linearity [27,28]. New interactions mediated by light mediators that couple electrons to neutrons generally lead to a nonlinear relation [25]. We shall denote such an effect as King linearity violation (KLV). The absence of a deviation from linearity allows us to constrain the NP contributions.

Existing measurements of isotope shifts cannot probe as-yet unconstrained regions of parameter space, but the projected sensitivity allows us to explore regions presently left unconstrained. The goal of this work is to investigate how this statement applies to specific models where couplings to other SM particles (in addition to the electron and neutron couplings) and thereby additional constraints become relevant.

The paper is organized as follows. In Sec. II we introduce the notation and provide a brief summary of Ref. [26]. In Sec. III we generalize the formalism and provide a fit of NP interactions to the available data sets of Ca^+ and Yb. As an application, we identify models for which KLV constraints are relevant, such as a new gauge boson Z'_{B-L}, the Higgs portal, chameleon models, and protophobic models in the context of the recently observed ^{8}Be anomaly, and we discuss the implications before concluding in Sec. V.

II. PROBING NEW PHYSICS VIA ISOTOPE SHIFT MEASUREMENTS

Consider a narrow atomic transition i between two atomic states and two even isotopes A and A'. The isotope shift (IS) is defined as the difference of the transition frequencies, $\nu_i^{AA'} \equiv \nu_i^A - \nu_i^{A'}$. The leading contributions to the IS stem from two sources: the mass shift (MS) and field shift (FS). The former arises from the mass difference of the isotopes A and A'. It can be factorized into an electronic coefficient K_i, which only depends on the transition i, and the isotope-dependent reduced mass given by

$$\mu_{AA'} = \frac{1}{m_A} - \frac{1}{m_{A'}}, \tag{1}$$

which is measured at high precision. The FS originates from the different volumes of the two isotopes. At leading order it also factorizes into the electronic, isotope-independent coefficient F_i and the charge radius variance, $\delta\langle r^2\rangle_{AA'} \equiv \langle r_A^2\rangle - \langle r_{A'}^2\rangle$, where r_A is the nuclear charge radius of isotope A. In contrast to $\mu_{AA'}$, $\delta\langle r^2\rangle_{AA'}$ is subject to large experimental uncertainties. The composition of the IS in terms of products of purely electronic and purely nuclear quantities is referred to as factorization [27]. As a result, these two leading contributions amount to the total IS as

$$\nu_i^{AA'} = K_i\mu_{AA'} + F_i\delta\langle r^2\rangle_{AA'} + \cdots, \tag{2}$$

where the first term represents the MS and the second one the FS [27,28]. The dots denote possible higher-order corrections and NP contributions which we will discuss below. It is useful to normalize the frequency shifts by the reduced mass $\mu_{AA'}$ to obtain the so-called modified isotope shifts, $m\nu_i^{AA'} \equiv \nu_i^{AA'}/\mu_{AA'}$, which we will use in the following. As a consequence, the mass shift is reduced to the electronic factor K_i whereas the FS factor F_i is multiplied by the modified charge radius variance, $m\delta\langle r^2\rangle_{AA'} \equiv \delta\langle r^2\rangle_{AA'}/\mu_{AA'}$.

When considering several pairs of isotopes, the modified Eq. (2) can be written in vectorial form as

$$\overrightarrow{m\nu}_i = K_i\overrightarrow{m\mu} + F_i\overrightarrow{m\delta\langle r^2\rangle}, \tag{3}$$

where each line corresponds to one set of isotopes. For the example of four isotopes combined to three isotope pairs $\{A, A_a\}$, where $a = 1, 2, 3$ and A is the reference isotope, the IS vector of transition i is given by $\overrightarrow{m\nu}_i = (m\nu_i^{AA_1}, m\nu_i^{AA_2}, m\nu_i^{AA_3})$, and $\overrightarrow{m\delta\langle r^2\rangle}$ accordingly. The mass shift vector is denoted by $\overrightarrow{m\mu} = (1, 1, 1)$.

With measurements of two transitions $i = 1, 2$ the unknown charge radius distribution can be replaced by measured quantities. Solving Eq. (3) with $i = 1$ for $\overrightarrow{m\delta\langle r^2\rangle}$ and replacing it in the equation with $i = 2$ leads to

$$\overrightarrow{m\nu}_2 = K_{21}\overrightarrow{m\mu} + F_{21}\overrightarrow{m\nu}_1, \tag{4}$$

with $F_{21} \equiv F_2/F_1$ and $K_{21} \equiv K_2 - F_{21}K_1$. Hence, this replacement gives rise to a linear dependence between the two sets of modified frequency shifts $\overrightarrow{m\nu}_{1,2}$, referred to as King linearity [27].

In order to quantify the observed linearity, we define a measure of nonlinearity [26],

$$\mathrm{NL} = (\overrightarrow{m\nu}_1 \times \overrightarrow{m\nu}_2)\cdot\overrightarrow{m\mu}, \tag{5}$$

which corresponds to the volume of the parallelepiped spanned by the vectors $\overrightarrow{m\nu}_1$, $\overrightarrow{m\nu}_2$, and $\overrightarrow{m\mu}$ (for illustration see Ref. [26]). King linearity is considered to hold if the measure NL is smaller than its uncertainty δNL.[1] In several atoms and ions, King linearity has indeed been established within the experimental uncertainty of $\sigma = 0.1$ MHz on the IS, see e.g. Refs. [30–34].

In Ref. [26] it was shown that new physics contributions from light bosons interacting with electrons and neutrons can lead to a deviation from the linear relation in Eq. (4). Thereby, the observation of linearity allows to set bounds on the mass and coupling of a possible new force mediator.

To be specific, a new physics contribution is added as a third term to Eq. (2),

$$\overrightarrow{m\nu}_i = K_i\overrightarrow{m\mu} + F_i\overrightarrow{m\delta\langle r^2\rangle} + y_e y_n X_i\vec{h}, \tag{6}$$

where y_e, y_n are the couplings of a new boson to electrons and neutrons, respectively. Furthermore, we have introduced the electronic NP factor X_i and the reduced isotope dependence $\vec{h}$. Both of them are model dependent; a specific expression is given below. Proceeding as in the SM case, one can express $\overrightarrow{m\nu}_2$ as a function of $\overrightarrow{m\nu}_1$, yielding

$$\overrightarrow{m\nu}_2 = K_{21}\overrightarrow{m\mu} + F_{21}\overrightarrow{m\nu}_1 + y_e y_n\vec{h}(X_2 - X_1F_{21}). \tag{7}$$

Thus, NP can break King linearity. For unit coupling, the NP contribution to NL is given by the projection of $\vec{h}$ onto the normal vector of the King plane,

$$\mathrm{NL}_{\mathrm{NP}} = [\overrightarrow{m\mu} \times (X_2\overrightarrow{m\nu}_1 - X_1\overrightarrow{m\nu}_2)]\cdot\vec{h}. \tag{8}$$

$\mathrm{NL}_{\mathrm{NP}}$ vanishes if

(i) NP mediates a short-range interaction, shorter than the nuclear size. In this case the electronic parameter X_i becomes proportional to the electronic parameter of the FS, namely $X_i \propto F_i$, so that the bracket in Eq. (7) vanishes or

(ii) the isotope-dependent NP contribution $\vec{h}$ is proportional either to $\overrightarrow{m\mu}$ or to the reduced charge radius $\overrightarrow{m\delta\langle r^2\rangle}$, such that the NP contribution can be absorbed in a redefinition of K_{21} or F_{21}, respectively.

Finally, solving the set of equations in Eq. (7) determines the central value of $y_e y_n$ needed to yield a particular data set $\{\overrightarrow{m\nu}_1, \overrightarrow{m\nu}_2, \overrightarrow{m\mu}\}$,

[1] At the present level of experimental accuracy, the uncertainties on the isotope masses are smaller by several orders of magnitude than those of the frequency shifts [e.g. $\mathcal{O}(10^{-5})$ smaller for Yb masses [29] with the present IS accuracy of 0.1–1 MHz [30,31]]. Therefore we will neglect them in our numerical evaluation. Once the uncertainties of IS measurements will be significantly reduced, the mass uncertainties will have to be taken into account.

$$y_e y_n = \frac{\mathrm{NL}}{\mathrm{NL}_{\mathrm{NP}}}. \tag{9}$$

The interval of $y_e y_n$ can be obtained via error propagation of the uncertainties on the involved quantities. In case of linearity, $y_e y_n$ is compatible with zero and the method reaches its maximal sensitivity, whereas if nonlinearity is found a bound can be set with the experimental resolution at which nonlinearity emerges. In the following we will adopt the same approach as in Ref. [26] based on the best-case projection where linearity holds up to the experimentally achievable precision.

Indeed, nonlinearity cannot only arise from NP, but also from SM higher-order contributions. The dominant effects are expected as corrections to the FS operator (see Refs. [35–39] for relevant discussions). However, these estimates are not tailored to the most promising elements and transitions. Thus, in order to fully exploit the KLV potential to probe NP interactions, a significant improvement of the atomic theory input will be crucial to match the experimental precision.

In the remainder of the paper, we will consider NP interactions that couple linearly to the SM fermions. Hence the isotope-dependent NP part takes the form

$$h_{AA'} = \frac{A - A'}{\mu_{AA'}} \simeq -AA' \,\mathrm{amu}, \tag{10}$$

where in the last step we approximated $m_A \simeq A\mathrm{amu}$ and amu denotes the atomic mass unit. Therefore, in this approximation, $\vec{h}$ can be written as $\vec{h} = -A\vec{A}'$ with $\vec{A}' = (A_1, A_2, A_3)$. We will further assume a Yukawa-like potential of the NP interaction, mediated by a boson ϕ of mass m_ϕ,

$$V_{\mathrm{NP}}(m_\phi, r) = \frac{y_e y_n}{4\pi}(A - Z)\frac{e^{m_\phi r}}{r}. \tag{11}$$

In the massless limit, $m_\phi \ll (1 + n_e)/a_0$ where a_0 is the Bohr radius and n_e the ionization number, the electronic NP factors X_i can be expressed as [26]

$$X_i|_{m_\phi = 0} \approx \frac{1}{2\pi\alpha}\left(\frac{E_b}{Z^b_{\mathrm{eff}}} - \frac{E_a}{Z^a_{\mathrm{eff}}}\right), \tag{12}$$

with α being the fine-structure constant. For the transition $i = a \to b$ between the energy levels E_a and E_b, the effective nuclear charges Z^ψ_{eff} account for the partial shielding of the nuclear charge for a valence electron at the states $\psi = a, b$, respectively. For later use, we define

$$x_i = X_i A \,\mathrm{amu}, \tag{13}$$

$$x_{ij} = x_i - F_{ij} x_j. \tag{14}$$

In the numerical evaluation in Sec. III we will use this Z_{eff} approximation; see Ref. [26] for more details.

III. FIT OF THE NP COUPLING

The formalism proposed in Ref. [26] and summarized in Sec. II is constructed for the minimal case of two transitions and three isotope pairs. However, at present there are already more measurements at comparable accuracy available in some systems, such as three transitions in Ca^+ [32,33] and four independent isotope pairs in Yb [30,31], see Table I. Hence the system is overconstrained and a fit of the NP coupling is necessary. In the following we will therefore perform a χ^2 fit to the data to obtain a limit on the NP coupling $y_e y_n$.

Under the assumptions made in Eqs. (10) and (12), Eq. (7) can be written for any two transitions i and j as

$$\overrightarrow{m\nu}_i = K_{ij}\overrightarrow{m\mu} + F_{ij}\overrightarrow{m\nu}_j + y_e y_n x_{ij}\vec{A}', \tag{15}$$

where x_{ij} is given in Eq. (14). This equation defines a family of parallel lines whose intercept depends on the new physics couplings $y_e y_n$ and the isotope pair via the third term. The lines live in the isotope shift space where each dimension corresponds to an isotope pair. When combining m transitions, we obtain for each isotope pair $\{A, A'\}$ a line in the m-dimensional space

$$\begin{pmatrix} m\nu_i^{AA'} \\ m\nu_j^{AA'} \\ \vdots \\ m\nu_m^{AA'} \end{pmatrix} = \begin{pmatrix} 0 \\ K_{ji} \\ \vdots \\ K_{mi} \end{pmatrix} + m\nu_i^{AA'} \begin{pmatrix} 1 \\ F_{ji} \\ \vdots \\ F_{mi} \end{pmatrix} + y_e y_n A' \begin{pmatrix} 0 \\ x_{ji} \\ \vdots \\ x_{mi} \end{pmatrix} \tag{16}$$

that can be fitted to the measured isotope shifts. For later convenience we write this equation as

$$\vec{P}^{AA'} = \vec{K} + m\nu_i^{AA'}\vec{F} + y_e y_n A'\vec{x}, \tag{17}$$

where the components of the above vectors follow from Eq. (16).

For the fit we construct a χ^2 function and marginalize over the entries of the vectors $\vec{K}$ and $\vec{F}$. Since the measured isotope shifts exhibit similar uncertainties in all transitions, a multidimensional χ^2 that includes the uncertainties of all transitions needs to be constructed (see e.g. Ref. [40]). For simplicity we assume that the uncertainties of the measurement are not correlated. In this case the contribution $\chi^2_{AA'}$ of the pair $\{A, A'\}$ to the χ^2 function is given by

$$\chi^2_{AA'} = \sum_i \left(\frac{d_i^{AA'}}{\sigma m\nu_i^{AA'}}\right)^2, \tag{18}$$

TABLE I. Measured transitions in Ca^+ and neutral Yb. λ denotes the wavelength of the transition in the reference isotope A, σ the experimental uncertainty on the isotope shifts, and n the number of available isotope pairs. In Ca^+, $A = 40$ is the reference isotope and $A' = 42,\ 44,\ 48$. In Yb, $A = 174$ and $A' = (168,)170, 172, 176$ for $n = 3(4)$. The Yb transitions with $\lambda =$ 404 nm and 408 nm are omitted in the fit due to their lower current resolution.

Element	Transition	λ(nm)	σ (MHz)	n	Ref.
Ca^+	$4S_{1/2} \to 4P_{1/2}$ (D1)	397	0.1	3	[32]
	$3D_{3/2} \to 4P_{1/2}$	866	0.1	3	[32]
	$4S_{1/2} \to 4P_{3/2}$ (D2)	393	0.1	3	[33]
Yb	$6^1S_0 \to 6^1P_1$	399	0.5	4	[30]
	$6^1S_0 \to 6^3P_1$	555.65	0.5	4	[31]
	$6^3D_2 \to 6^1S_0$	404	10	3	[34]
	$6^3D_1 \to 6^1S_0$	408	2	3	[34]

where the sum runs over all transitions. Here, $\sigma m\nu_i^{AA'}$ is the uncertainty of the respective IS measurement, and $d_i^{AA'}$ is the ith component of the vector connecting the measured point $\vec{P}^{AA'} = (m\nu_i^{AA'}, m\nu_j^{AA'}, \ldots, m\nu_m^{AA'})$ to the line defined by Eq. (16),

$$\vec{d}^{AA'} = (\vec{P}^{AA'} - \vec{c}_0^{AA'}) - \hat{n} \cdot [\hat{n} \cdot (\vec{P}^{AA'} - \vec{c}_0^{AA'})], \quad (19)$$

with $\vec{c}_0^{AA'} = \vec{K} + y_e y_n A' \vec{x}$ and $\hat{n} = \vec{F}/|\vec{F}|$. The full χ^2 function is given by summing over all isotope pairs.

By construction, the IS of the transition that appears in the right-hand side of Eq. (16) seemingly has a special role. This is, however, not the case as the distance between a point and a line in an m-dimensional space is invariant under the permutation of coordinates. When minimizing the χ^2 we have checked the consistency of our computation and its numerical stability by verifying that all permutations of the isotope shifts yield comparable results. We obtain the 95% confidence level limits on $y_e y_n$ shown in Table II. The near degeneracy between two of the transitions in Ca^+ is reflected in the extremely weak limit in the case of omitting the nondegenerate transition of $\lambda = 866$ nm. Moreover, this explains why the limit hardly becomes more stringent when including all three transitions. For Yb the limits get in general weaker by a factor $\mathcal{O}(1)$ to $\mathcal{O}(10)$ when one isotope shift measurement is dropped. The removal of $A' = 172$ leads to the weakest bound.

Omitting one transition of Ca^+ or one isotope pair of Yb leads to the minimal case of $m = 2$ transitions and $n = 3$ isotope pairs where Eq. (15) is exactly solvable. Hence, the theory parameters F_{21}, K_{21}, and $y_e y_n$ can be chosen such that the theory predictions of the modified isotope shifts reproduce exactly the measured ones. This is reflected by the vanishing χ^2_{min} in Table II.

IV. IMPLICATIONS FOR BSM MODELS

In Ref. [26] the sensitivity of KLV was compared to other measurements in a model-independent way. In the following we will translate the KLV bounds into bounds on the parameters of various BSM models and compare them to existing constraints. In addition we will explore the sensitivity of the near-future KLV projections with Ca^+ D-states, Sr^+, Sr/Sr^+, and Yb^+ as reported in Ref. [26]. We focus on those models that can be best probed by KLV measurements. While we discuss in detail the various constraints on the $B - L$ model in the full mass range relevant for KLV, we highlight promising mass values in Higgs portal and chameleon models. Most bounds on the $B - L$ model can be translated also to these models by rescaling. Furthermore, we present updated bounds on the protophobic interpretation of the Be anomaly.

A. Z' vector boson from $U(1)_{B-L}$

One of the frequently studied abelian extensions of the SM gauge group is gauging the difference of baryon and lepton number, $B - L$. Under this additional interaction all quarks therefore have the same charge, $z_q = 1/3$, and all leptons $z_l = -1$. The group is made anomaly free by introducing a right-handed neutrino for each family. In this model, the coupling g_{B-L} of the new vector boson Z' is

TABLE II. Minimal value of χ^2 as well as upper and lower 95% C.L. bounds and the best-fit value of the product of the couplings as determined by the fit for $m_\phi = 0$.

Element	Omitting	$y_e y_n\|_{\text{min}}$	$y_e y_n\|_{\text{best}}$	$y_e y_n\|_{\text{max}}$	χ^2_{min}
Ca^+	397 nm	-2.8×10^{-9}	-6.7×10^{-10}	$+1.3 \times 10^{-9}$	0.00
	866 nm	-9.2	$+1.0$	$+8.8$	0.00
	393 nm	-2.8×10^{-9}	-6.1×10^{-10}	$+1.5 \times 10^{-9}$	0.00
	⋯	-2.8×10^{-9}	-6.4×10^{-10}	$+1.3 \times 10^{-9}$	0.04
Yb	168	-2.8×10^{-9}	-9.3×10^{-10}	$+9.9 \times 10^{-10}$	0.00
	170	-2.6×10^{-9}	-7.6×10^{-10}	$+1.1 \times 10^{-9}$	0.00
	172	-2.8×10^{-8}	$+1.2 \times 10^{-8}$	$+6.5 \times 10^{-8}$	0.00
	176	-1.9×10^{-8}	-5.1×10^{-9}	$+9.7 \times 10^{-9}$	0.00
	⋯	-2.6×10^{-9}	-8.1×10^{-10}	$+1.1 \times 10^{-9}$	0.34

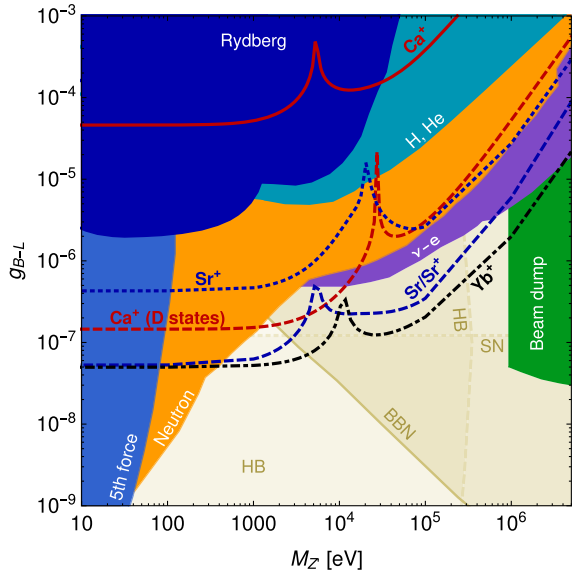

FIG. 1. Constraints on a Z' gauge boson from $U(1)_{B-L}$. KLV bound from existing IS data: Ca^+ with uncertainty $\sigma \simeq 0.1$ MHz (397 nm vs 866 nm [32], solid red line). KLV projections for $\sigma = 1$ Hz assuming linearity in Ca^+ ($S \to D$ transitions, red, dashed), Sr^+ (blue, dotted), Sr/Sr^+ (blue, dashed), and Yb^+ (black, dash-dotted) [26]. For comparison, bounds from fifth-force searches via the Casimir effect [44,45] (blue), neutron scattering [46–48] (orange), Rydberg states [49–51] (dark blue), energy level shifts in H and He [11] (turquoise), $\nu - e$ scattering at GEMMA and Borexino [41] (purple), and beam dump experiments [2,3,52] (green). Astrophysical and cosmological probes (beige): supernova 1987A with $\mathcal{O}(1)$ uncertainties [53–55] (SN, the area below the dotted line), horizontal branch stars [53,56–59] (HB, the area left of the dashed line) and Big Bang nucleosynthesis (BBN) via $N_{\rm eff}$ [42,60] (the area above the solid line).

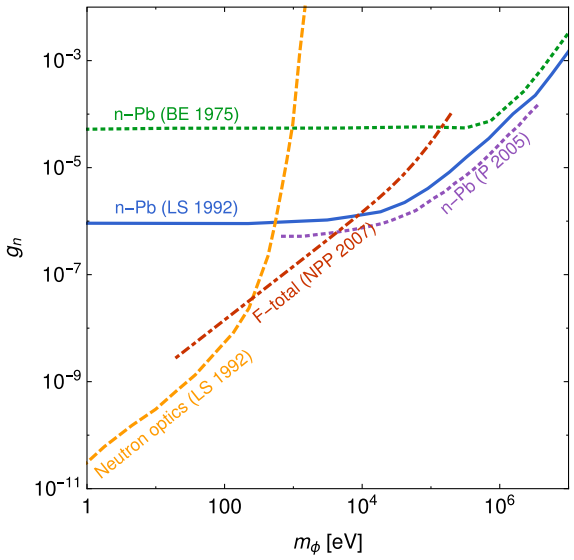

FIG. 2. Existing bounds on the neutron coupling g_n of a new boson ϕ from the neutron-electron scattering length in Pb, Bi, and noble gases denoted as neutron optics [46] (orange, dashed); n-^{208}Pb scattering at neutron energies of $E_n \sim 1$–26 keV [61] (green, dotted), 10 eV–10 keV [46] (blue, solid) and up to 20 keV including interference of resonant and nonresonant amplitudes [48] (purple, dotted); and the comparison of the total to the forward-scattering cross section of neutrons on nuclei [47] (red, dash-dotted). For discussion see Sec. IV A 1.

purely vectorial and of equal strength for electrons and neutrons; hence, KLV is a promising method to probe this kind of NP interaction.

In Fig. 1 we compare the KLV bounds and projections from different atoms and ions to existing constraints in the mass range of $M_{Z'} \sim 10$ eV to a few MeV. For other overviews collecting bounds on this model and related models see e.g. Refs. [11,41–43].

1. Laboratory bounds

The existence of a fifth force is severely constrained for a mass $M_{Z'} \lesssim 100$ eV by experiments testing the Casimir effect [44,45].

In contrast to KLV, other atomic precision measurements such as energy level shifts in Rydberg states [49–51] and in s- and p-states of atomic H and hydrogenlike He^+ [11] provide bounds on $y_p y_e$ where y_p is the proton coupling. In the massless limit, $M_{Z'} \ll (1 + n_e)/a_0$, the NP potential probed by these observables simplifies to a Coulomb potential. In this case the NP interaction is absorbed by a redefinition of the fine-structure constant α, resulting in a weakening of the bounds. Due to its sensitivity to $y_e y_n$, KLV is not affected by this redefinition, so that its bound remains constant in the massless limit and is the strongest among the atomic spectroscopy bounds for mediator masses below 0.3 eV. The intersection of the Ca^+ and Rydberg bound was determined following Ref. [51] and lies below the mass range shown in Fig. 1. Yet, one needs to keep in mind that for $M_{Z'} \leq 0.3$ eV also other constraints apply, such as from the Casimir effect mentioned above or from tests for a deviation from the Coulomb force, see e.g. Ref. [43].

Neutron scattering is a powerful probe of the interaction between new bosons and neutrons over a wide mass range. Among the neutron-scattering experiments, neutron optics [46] provides the strongest constraint on g_n, in this model equivalent to g_{B-L}, in the mass range of $M_{Z'} \lesssim 500$ eV. For 500 eV $\lesssim M_{Z'} \lesssim 5$ keV, the comparison of the total to the forward-scattering cross section [47] is most sensitive. Above $M_{Z'} \sim 5$ keV, the neutron-lead (n-Pb) scattering [48] sets the strongest bound. This method is based on the proposal by Ref. [61] whose bounds are superseded by the ones reported in Refs. [46,48]. The collection of the various bounds is shown in Fig. 2; the limit presented in Fig. 1 shows the best bound for each mass. When comparing to KLV, the considerable uncertainties on the neutron-scattering bounds need to be kept in mind [47,62–64]. In particular, the uncertainties related to the electron-neutron

scattering length, various nuclear inputs, and the missing higher-order terms in the neutron-scattering cross section are not easy to determine precisely. Similarly, the bounds inferred for masses far higher than the neutron energies of $E_n \sim 10$ keV [46] are also subject to large uncertainties. In addition, in the derivation of the various neutron bounds it is assumed that the NP contribution to the neutron-electron interaction is either absorbed in the corresponding measurement of the neutron-electron scattering length, b_{ne}, or negligible [47].

For masses above a few keV, the neutron bounds are exceeded by constraints that arise from measurements of neutrino-electron $(\nu - e)$ scattering. Measurements from Borexino [65] and GEMMA [66] have been interpreted in the $B - L$ model in Ref. [41] and are the strongest laboratory bounds between 4 keV and 1 MeV.

The limit on g_{B-L} via g_e from the bound on the anomalous magnetic moment of the electron, $(g-2)_e$, is less constraining than the neutron-scattering bounds in the same mass range [67]; thus, we omit it in Fig. 1.

Above the electron threshold, i.e. $M_{Z'} \gtrsim 1$ MeV, and up to $M_{Z'} \lesssim 100$ MeV, high-intensity electron and proton beam dump experiments [2,3,52] provide the strongest bound on g_{B-L}. For a review see Ref. [1] and references therein.

2. Astrophysical and cosmological bounds

A large part of the parameter space of a new light boson interacting with SM fermions is constrained by astrophysical probes. In particular, bounds on the cooling rate in horizontal branch stars limit the coupling of Z' as long as its mass is within the thermal reach ($M_{Z'} \lesssim 350$ keV) [53,56–59]. Here we omit the corresponding bound from sun cooling since its excluded region is also covered by the horizontal branch stars. Furthermore, the energy loss in the core of the supernova SN 1987A constrains the neutron coupling for masses of $M_{Z'} \lesssim 100$ MeV [53,54], though with large uncertainties [55].

The coupling g_{B-L} is also severely constrained by the effective number of neutrinos N_{eff} [42,60]. If a light mediator couples to neutrinos, it can thermalize via the inverse decay $\nu + \bar{\nu} \to Z'$ or $\nu + \bar{\nu} \to Z'Z'$, thus contributing to the energy density of the Universe. The first process dominates for $1\ \text{eV} \lesssim M_{Z'} \lesssim 1$ MeV, and the second one for $M_{Z'} \ll 1$ eV. Under the requirement that the NP contribution to N_{eff}, Δ_ν, fulfills $\Delta_\nu < 1$ at $T = 1$ MeV, a large parameter region is excluded.

Although the cosmological and astrophysical bounds exceed all KLV projections, a complementary laboratory probe of this region will nevertheless be valuable, in particular because isotope shifts are a very clean observable and the derived bounds are based on less model assumptions. For example, the constraint from Δ_ν can be avoided by charging only the right-handed electrons under the new gauge group. However, in such a model other strong constraints arise, for instance, from the cancellation of a gauge anomaly in the case of an anomalous gauge group [68]. For examples of UV-complete models of axial couplings with such phenomenology, see Refs. [69,70]. Moreover, in this class of models the axial coupling $g_A^e \neq 0$. In presence of an axial coupling to electrons and vectorial couplings to quarks, atomic parity violation (APV) [71] is a more sensitive probe than KLV. For instance, for gauge bosons with $m_{Z'} \sim 0.1$ MeV, the limit from APV [71] is several orders of magnitude stronger than the Yb^+ projection. The same conclusion is obtained for constraints on the mixing of a new light gauge boson Z' with the SM Z [72].

3. KLV bounds and projections

Due to the simple coupling structure of the Z' boson, the limits from KLV are straightforwardly obtained from Ref. [26] by identifying $g_{B-L}^2 = y_e y_n$. The existing bound from Ca^+ is shown by the solid red line, the projections are shown by dashed lines. While the existing bound does not compete with other laboratory bounds, the projected bounds will extend the reach of laboratory bounds in the mass range of $300\ \text{eV} \lesssim M_{Z'} \lesssim 1$ MeV, in particular using Sr/Sr^+ and Yb^+. Hence, KLV has the potential to put the regions that are currently only probed by astrophysical and cosmological observables under scrutiny.

B. Higgs portal

Another example for a new light mediator which gives rise to a spin-independent interaction between electrons and neutrons is a scalar singlet mixed with the Higgs boson [73,74]. This model can be linked to the solution of the hierarchy problem via the relaxion mechanism, where the relaxion takes the role of the new scalar that mixes with the Higgs boson [10,75].

We evaluate the KLV sensitivity to this class of models for a very light scalar ϕ with mass $m_\phi \lesssim 5$ keV. In this case the KLV bound on the mixing angle $\theta_{h\phi}$ between the singlet and the Higgs boson is given by

$$\sin^2\theta_{h\phi} \lesssim 2 \times 10^{-6} \cdot \left[\frac{4 \times 10^{-9}}{y_e y_n}\right] \frac{\sigma}{\text{Hz}}, \tag{20}$$

where we assumed the strongest KLV projections for this mass given in Ref. [26], i.e. Yb^+ with a precision σ at the 1 Hz level. The quark and gluon contribution to the neutron Yukawa coupling can be obtained using Refs. [76–78]. For SM Yukawa couplings, the limit from neutron scattering is stronger by 1 order of magnitude since the KLV observable depends on the electron Yukawa coupling that is much smaller than the neutron Yukawa coupling. Yet, for models where the electron (neutron) coupling is enhanced (suppressed) by at least 1 order of magnitude with respect to its SM value, KLV could set a stronger bound than neutron scattering. For assumptions regarding the bound from

neutron scattering see Sec. IV A 1. Under these assumptions and if the electron (neutron) coupling is enhanced (suppressed) by a factor of ∼10, KLV sets a stronger bound than neutron scattering for $m_\phi \gtrsim 30$ keV and the strongest bound of all in the region 350 keV $\lesssim m_\phi \lesssim 1$ MeV. Below this range a stronger bound arises from horizontal branch stars [53,56–59] and above 1 MeV beam dump experiments are more constraining.

A suppressed y_n can arise for example in less minimal Higgs portal models, such as the leptonic Higgs portal [79]. In this model, the singlet ϕ couples to leptons with a similar strength as the 125 GeV Higgs boson, i.e. $y_l^\phi \sim \frac{m_l}{v}$, while its coupling to the quarks is suppressed compared to normal Higgs portal scenarios; hence, neutron-scattering experiments lose sensitivity.

C. Chameleon models

The chameleon is a scalar field ϕ with an effective potential that depends on the density ρ of the environment [80,81]

$$V_{\text{eff}} = V(\phi) + \frac{\phi\rho}{M}, \tag{21}$$

with M being a mass scale characterizing the coupling of the chameleon to matter, and $V(\phi)$ is chosen such that the mass of ϕ increases with increasing ρ. As a result the mass of the scalar is heavy in a dense environment and light otherwise, which leads to a screening effect in test masses. Therefore it can mediate a long-range force on cosmological scales but avoid constraints from fifth-force experiments.

On atomic scales the chameleon can alter the energy levels of the electrons. The relevant part of the NP perturbation of the Hamiltonian that can be probed by KLV is given by [82,83]

$$\delta H|_n = -\frac{m_e m_N}{4\pi r M^2}, \tag{22}$$

where m_e is the electron mass, $m_N \simeq (A-Z)m_n$ the contribution of the neutrons to the nucleus mass, and r the distance to the nucleus. In this expression we omit a possible screening of the nucleus as it depends not only on the parameter space of the model but also on the experimental setup [84].

Assuming the massless case, Eq. (22) can be matched to Eq. (11) and the bounds on $y_e y_n$ can be easily translated into bounds on M

$$M > \sqrt{\frac{m_e m_n}{y_e y_n|_{\text{min}}}} \approx 500 \text{ TeV} \approx 2.5 \times 10^{-13}\, M_{\text{Pl}}, \tag{23}$$

where M_{Pl} is the reduced Planck mass and we used the Yb^+ KLV projection. This is stronger by more than an order of magnitude than the current best bound from measurements of energy levels in hydrogen and helium atoms [11,85,86], which leads to a bound of $M \gtrsim 10$ TeV [87]. Depending on the parameter space, this can even be the strongest bound on M. The current bound of 10 TeV is stronger than the present KLV bound from Ca^+ and Yb.

D. Beryllium anomaly

Recently, a 6.8σ anomaly was reported in rare nuclear decays of ^{8}Be [88]. The anomaly arises in the isoscalar transition $^8\text{Be}^*(1^+) \to {}^8\text{Be}(0^+) + e^+e^-$ as a bump in the distribution of the opening angle of the emitted electron-positron pairs. This observation can be explained by the emission of a particle X with mass $m_X \approx 17$ MeV in the process $^8\text{Be}^*(1^+) \to {}^8\text{Be}(0^+) + X$, which subsequently decays into an electron positron pair. The best agreement with observations is obtained for X being a vector with either axial or vectorial couplings to quarks and electrons [69,70,89,90]. It was noted in Refs. [89,90] that the vectorlike interpretation necessitates protophobic couplings to quarks, or else it would be in conflict with other observables. Therefore KLV can provide the necessary method to confirm or reject this hypothesis.

In Fig. 3 we present KLV projections and compare them to existing bounds on y_e and y_n for a fixed mass of $m_X = 17$ MeV. The gray shaded area corresponds to the range of the couplings that explains the observed excess and is not in conflict with other measurements.

The upper bound on y_e comes from $(g-2)_e$ measurements. In contrast to Refs. [89,90] the plotted bound

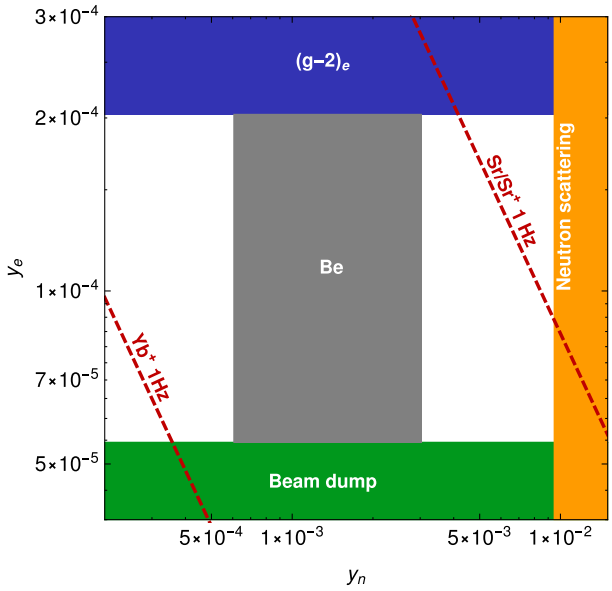

FIG. 3. Bounds of 95% C.L. on y_e and y_n for a protophobic vector boson of mass $m_X = 17$ MeV. The gray region represents the required and allowed couplings to explain the ^{8}Be anomaly. The dashed lines show the projected upper bounds on the couplings from KLV measurements in Sr/Sr^+ and Yb^+.

represents the 95% C.L. instead of the 3σ limit. Another upper bound is provided by KLOE-2 [91]. However even this 90% C.L. bound is weaker than the 95% C.L. bound from the magnetic moment and therefore not shown. The lower bound on y_e stems from beam dump experiments requiring that the new particle decays before it leaves the detector. The strongest bound for $m_X = 17$ MeV is provided by the E141 experiment [92] and interpreted in Ref. [52]. The latter corrected Ref. [2] that was used in Refs. [89,90].

An upper bound on y_n is set by neutron-Pb scattering. The strongest constraint for $m_X = 17$ MeV is provided by Ref. [46] which is stronger than the older one derived in Ref. [61] and used in Refs. [89,90]. The bound shown in Fig. 3 is weaker by a factor of $\sqrt{A/(A-Z)}$ than the one presented in Fig. 2 due to the protophobic nature of the coupling. In contrast to the neutron scattering, KLV does not lose sensitivity in the protophobic case.

The dashed lines show the projected upper bounds of KLV on the product of the couplings $y_e y_n$, assuming linearity. While Sr/Sr^+ will not suffice to probe the couplings relevant for the Be anomaly, Yb^+ has the potential to exclude or support the existence of a new vector with a mass of $m_X = 17$ MeV. With a precision of $\mathcal{O}(30\ \text{Hz})$ Yb^+ will become sensitive to the relevant Be coupling space and with the anticipated precision of 1 Hz the whole region can be covered.

V. CONCLUSIONS

In this work we extended the proposal of Ref. [26] to constrain NP by means of isotope shift spectroscopy to enable the inclusion of larger data sets with an arbitrary number of atomic transitions and isotope pairs. As an application of the KLV observable to bound NP couplings, we evaluated the constraints resulting from existing data sets of two different atomic systems (Ca^+ and Yb).

We compare the existing KLV bounds and near-future projections to present constraints in various models that can potentially be probed by isotope shifts.

(i) $B-L$: The $M_{Z'} - g_{B-L}$ space is already largely constrained by astrophysical and cosmological bounds. Complementary laboratory probes, however, are not yet able to confirm those bounds in certain areas of the parameter space. Here KLV has the potential to become the strongest laboratory bound for $300\ \text{eV} \lesssim M_{Z'} \lesssim 1$ MeV.

(ii) Higgs portal: While KLV bounds on standard Higgs portals are weaker than existing laboratory bounds, KLV can supersede them in the case of an enhanced electron or suppressed neutron coupling. For an enhancement (suppression) by a factor of 10, KLV could even set the strongest of all bounds in the range $350\ \text{keV} \lesssim m_\phi \lesssim 1$ MeV. Such a scenario can be realized e.g. in the leptonic Higgs portal.

(iii) Chameleon: KLV will be able to set the strongest lower bound $M > 500$ TeV on the interaction scale of the chameleon with matter.

(iv) Be anomaly: With the anticipated precision, KLV will fully explore the coupling range of a protophobic vector boson with mass $m_X = 17$ MeV needed to reproduce the observed anomaly in ^{8}Be decays.

ACKNOWLEDGMENTS

We thank Cedric Delaunay and Yotam Soreq for useful discussions and for carefully reading our draft. The work of G. P. is supported by grants from the United States-Israel Binational Science Foundation, European Research Council, Israeli Science Foundation, Minerva, and the Weizmann-UK Making Connections Programme.

[1] J. Alexander *et al.*, in Dark sectors 2016 workshop: Community report, arXiv:1608.08632.
[2] R. Essig, P. Schuster, and N. Toro, Probing dark forces and light hidden sectors at low-energy $e+e-$ colliders, Phys. Rev. D **80**, 015003 (2009).
[3] R. Essig, P. Schuster, N. Toro, and B. Wojtsekhowski, An electron fixed target experiment to search for a new vector boson A' decaying to $e+e-$, J. High Energy Phys. 02 (2011) 009.
[4] B. Batell, M. Pospelov, and A. Ritz, Probing a secluded U(1) at B-factories, Phys. Rev. D **79**, 115008 (2009).
[5] B. Batell, M. Pospelov, and A. Ritz, Exploring portals to a hidden sector through fixed targets, Phys. Rev. D **80**, 095024 (2009).
[6] E. Izaguirre, G. Krnjaic, P. Schuster, and N. Toro, Physics motivation for a pilot dark matter search at Jefferson Laboratory, Phys. Rev. D **90**, 014052 (2014).
[7] B. A. Dobrescu and C. Frugiuele, GeV-Scale dark matter: Production at the main injector, J. High Energy Phys. 02 (2015) 019.
[8] P. Coloma, B. A. Dobrescu, C. Frugiuele, and R. Harnik, Dark matter beams at LBNF, J. High Energy Phys. 04 (2016) 047.
[9] C. Frugiuele, Probing sub-GeV dark sectors via high energy proton beams at LBNF/DUNE and MiniBooNE, arXiv:1701.05464.
[10] T. Flacke, C. Frugiuele, E. Fuchs, R. S. Gupta, and G. Perez, Phenomenology of relaxion-Higgs mixing, J. High Energy Phys. 06 (2017) 050.

[11] J. Jaeckel and S. Roy, Spectroscopy as a test of Coulomb's law: A probe of the hidden sector, Phys. Rev. D **82**, 125020 (2010).
[12] F. Ficek, D. F. J. Kimball, M. Kozlov, N. Leefer, S. Pustelny, and D. Budker, Constraints on exotic spin-dependent interactions between electrons from helium fine-structure spectroscopy, Phys. Rev. A **95**, 032505 (2017).
[13] S. G. Porsev, K. Beloy, and A. Derevianko, Precision Determination of Electroweak Coupling from Atomic Parity Violation and Implications for Particle Physics, Phys. Rev. Lett. **102**, 181601 (2009).
[14] K. Tsigutkin, D. Dounas-Frazer, A. Family, J. E. Stalnaker, V. V. Yashchuk, and D. Budker, Observation of a Large Atomic Parity Violation Effect in Ytterbium, Phys. Rev. Lett. **103**, 071601 (2009).
[15] K. Tsigutkin, D. Dounas-Frazer, A. Family, J. E. Stalnaker, V. V. Yashchuk, and D. Budker, Parity violation in atomic ytterbium: Experimental sensitivity and systematics, Phys. Rev. A **81**, 032114 (2010).
[16] N. Leefer, L. Bougas, D. Antypas, and D. Budker, Towards a new measurement of parity violation in dysprosium, in *Proceedings of PAVI2014* (2014), arXiv:1412.1245.
[17] O. O. Versolato *et al.*, Atomic parity violation in a single trapped radium ion, Hyperfine Interact. **199**, 9 (2011).
[18] V. A. Dzuba, J. C. Berengut, V. V. Flambaum, and B. Roberts, Revisiting Parity Nonconservation in Cesium, Phys. Rev. Lett. **109**, 203003 (2012).
[19] B. M. Roberts, V. A. Dzuba, and V. V. Flambaum, Parity and time-reversal violation in atomic systems, Annu. Rev. Nucl. Part. Sci. **65**, 63 (2015).
[20] K. P. Jungmann, Symmetries and fundamental interactions-selected topics, Hyperfine Interact. **227**, 5 (2014).
[21] V. A. Dzuba, V. V. Flambaum, M. S. Safronova, S. G. Porsev, T. Pruttivarasin, M. A. Hohensee, and H. Höffner, Strongly enhanced effects of Lorentz symmetry violation in entangled Yb^+ ions, arXiv:1507.06048.
[22] V. V. Flambaum, Enhanced effects of the Lorentz invariance and Einstein equivalence principle violation in 229Th nuclear transition, arXiv:1511.04848.
[23] R. Godun, P. Nisbet-Jones, J. Jones, S. King, L. Johnson, H. Margolis, K. Szymaniec, S. Lea, K. Bongs, and P. Gill, Frequency Ratio of Two Optical Clock Transitions in $^{171}Yb^+$ and Constraints on the Time Variation of Fundamental Constants, Phys. Rev. Lett. **113**, 210801 (2014).
[24] T. Rosenband, D. B. Hume, P. O. Schmidt, C. W. Chou, A. Brusch, L. Lorini, W. H. Oskay, R. E. Drullinger, T. M. Fortier, J. E. Stalnaker, S. A. Diddams, W. C. Swann, N. R. Newbury, W. M. Itano, D. J. Wineland, and J. C. Bergquist, Frequency ratio of Al^+ and Hg^+ single-ion optical clocks; Metrology at the 17th decimal place, Science **319**, 1808 (2008).
[25] C. Delaunay, R. Ozeri, G. Perez, and Y. Soreq, Probing the atomic Higgs force, arXiv:1601.05087.
[26] J. C. Berengut *et al.*, Probing new light force-mediators by isotope shift spectroscopy, arXiv:1704.05068.
[27] W. H. King, Comments on article peculiarities of isotope shift in samarium spectrum, J. Opt. Soc. Am. **53**, 638 (1963).
[28] W. H. King, *Isotope Shifts in Atomic Spectra* (Plenum Press, New York, 1984).
[29] E. G. Myers, The most precise atomic mass measurements in Penning traps, Int. J. Mass Spectrom. **349–350**, 107 (2013).
[30] M. Kleinert, M. E. Gold Dahl, and S. Bergeson, Measurement of the Yb I $^1S_0 - {}^1P_1$ transition frequency at 399 nm using an optical frequency comb, Phys. Rev. A **94**, 052511 (2016).
[31] D. L. Clark, M. E. Cage, D. A. Lewis, and G. W. Greenlees, Optical isotopic shifts and hyperfine splittings for Yb, Phys. Rev. A **20**, 239 (1979).
[32] F. Gebert, Y. Wan, F. Wolf, C. N. Angstmann, J. C. Berengut, and P. O. Schmidt, Precision Isotope Shift Measurements in Calcium Ions Using Quantum Logic Detection Schemes, Phys. Rev. Lett. **115**, 053003 (2015).
[33] C. Shi, F. Gebert, C. Gorges, S. Kaufmann, W. Nörtershäuser, B. K. Sahoo, A. Surzhykov, V. A. Yerokhin, J. C. Berengut, F. Wolf, J. C. Heip, and P. O. Schmidt, Unexpectedly large difference of the electron density at the nucleus in the $4p^2P_{1/2,3/2}$ fine-structure doublet of Ca^+, Appl. Phys. B **123**, 2 (2017).
[34] C. J. Bowers, D. Budker, S. J. Freedman, G. Gwinner, J. E. Stalnaker, and D. DeMille, Experimental investigation of the $6s^2{}^1S_0 \rightarrow 5d6s^3D_{1,2}$ forbidden transitions in atomic ytterbium, Phys. Rev. A **59**, 3513 (1999).
[35] C. W. P. Palmer and D. N. Stacey, Theory of anomalous isotope shifts in samarium, J. Phys. B **15**, 997 (1982).
[36] E. C. Seltzer, *K* X-ray isotope shifts, Phys. Rev. **188**, 1916 (1969).
[37] J. A. R. Griffith, G. R. Isaak, R. New, and M. P. Ralls, Anomalies in the optical isotope shifts of samarium, J. Phys. B **14**, 2769 (1981).
[38] S. A. Blundell, P. E. G. Baird, C. W. P. Palmer, D. N. Stacey, and G. K. Woodgate, A reformulation of the theory of field isotope shift in atoms, J. Phys. B **20**, 3663 (1987).
[39] G. Torbohm, B. Fricke, and A. Rosén, State-dependent volume isotope shifts of low-lying states of group-IIa and -IIb elements, Phys. Rev. A **31**, 2038 (1985).
[40] D. W. Hogg, J. Bovy, and D. Lang, Data analysis recipes: Fitting a model to data, arXiv:1008.4686.
[41] R. Harnik, J. Kopp, and P. A. N. Machado, Exploring ν signals in dark matter detectors, J. Cosmol. Astropart. Phys. 07 (2012) 026.
[42] J. Heeck, Unbroken $B - L$ symmetry, Phys. Lett. B **739**, 256 (2014).
[43] J. Jaeckel and A. Ringwald, The low-energy frontier of particle physics, Annu. Rev. Nucl. Part. Sci. **60**, 405 (2010).
[44] M. Bordag, U. Mohideen, and V. M. Mostepanenko, New developments in the Casimir effect, Phys. Rep. **353**, 1 (2001).
[45] M. Bordag, G. L. Klimchitskaya, U. Mohideen, and V. M. Mostepanenko, *Advances in the Casimir Effect*, International Series of Monographs on Physics Vol. 145 (Oxford University Press, New York, 2009).
[46] H. Leeb and J. Schmiedmayer, Constraint on Hypothetical Light Interacting Bosons from Low-Energy Neutron Experiments, Phys. Rev. Lett. **68**, 1472 (1992).
[47] V. V. Nesvizhevsky, G. Pignol, and K. V. Protasov, Neutron scattering and extra short range interactions, Phys. Rev. D **77**, 034020 (2008).

[48] Yu. N. Pokotilovski, Constraints on new interactions from neutron scattering experiments, Phys. At. Nucl. **69**, 924 (2006).
[49] D. F. Bartlett and S. Lögl, Limits on an Electromagnetic Fifth Force, Phys. Rev. Lett. **61**, 2285 (1988).
[50] S. G. Karshenboim, Precision Physics of Simple Atoms and Constraints on a Light Boson with Ultraweak Coupling, Phys. Rev. Lett. **104**, 220406 (2010).
[51] S. G. Karshenboim, Constraints on a long-range spin-independent interaction from precision atomic physics, Phys. Rev. D **82**, 073003 (2010).
[52] S. Andreas, C. Niebuhr, and A. Ringwald, New limits on hidden photons from past electron beam dumps, Phys. Rev. D **86**, 095019 (2012).
[53] W. M. Yao *et al.* (Particle Data Group Collaboration), Review of particle physics, J. Phys. G **33**, 1 (2006).
[54] G. Raffelt, Limits on a *CP*-violating scalar axion-nucleon interaction, Phys. Rev. D **86**, 015001 (2012).
[55] K. Blum and D. Kushnir, Neutrino signal of collapse-induced thermonuclear supernovae: The case for prompt black hole formation in SN1987A, Astrophys. J. **828**, 31 (2016).
[56] J. A. Grifols and E. Masso, Constraints on finite range baryonic and leptonic forces from stellar evolution, Phys. Lett. B **173**, 237 (1986).
[57] J. A. Grifols, E. Masso, and S. Peris, Energy loss from the sun and red giants: Bounds on short range baryonic and leptonic forces, Mod. Phys. Lett. A **04**, 311 (1989).
[58] E. Hardy and R. Lasenby, Stellar cooling bounds on new light particles: Plasma mixing effects, J. High Energy Phys. 02 (2017) 033.
[59] J. Redondo and G. Raffelt, Solar constraints on hidden photons re-visited, J. Cosmol. Astrophys. Part. 08 (**2013**) 034.
[60] B. Ahlgren, T. Ohlsson, and S. Zhou, Comment on "Is Dark Matter with Long-Range Interactions a Solution to All Small-Scale Problems of Λ Cold Dark Matter Cosmology, Phys. Rev. Lett. **111**, 199001 (2013).
[61] R. Barbieri and T. E. O. Ericson, Evidence against the existence of a low mass scalar boson from neutron-nucleus scattering, Phys. Lett. **57B**, 270 (1975).
[62] F. Wissmann, M. Schumacher, and M. I. Levchuk, On approaches to measure the electromagnetic polarizabilities of the neutron, Eur. Phys. J. A **1**, 193 (1998).
[63] I. Antoniadis *et al.*, Short-range fundamental forces, C.R. Phys. **12**, 755 (2011).
[64] D. Tucker-Smith and I. Yavin, Muonic hydrogen and MeV forces, Phys. Rev. D **83**, 101702 (2011).
[65] G. Bellini *et al.*, Precision Measurement of the 7Be Solar Neutrino Interaction Rate in Borexino, Phys. Rev. Lett. **107**, 141302 (2011).
[66] A. G. Beda, E. V. Demidova, A. S. Starostin, V. B. Brudanin, V. G. Egorov, D. V. Medvedev, M. V. Shirchenko, and T. Vylov, GEMMA experiment: Three years of the search for the neutrino magnetic moment, Phys. Part. Nucl. Lett. **7**, 406 (2010).
[67] D. Hanneke, S. Fogwell, and G. Gabrielse, New Measurement of the Electron Magnetic Moment and the Fine Structure Constant, Phys. Rev. Lett. **100**, 120801 (2008).
[68] B. A. Dobrescu and C. Frugiuele, Hidden GeV-Scale Interactions of Quarks, Phys. Rev. Lett. **113**, 061801 (2014).
[69] J. Kozaczuk, D. E. Morrissey, and S. R. Stroberg, Light axial vectors, nuclear transitions, and the ^{8}Be anomaly, Phys. Rev. D **95**, 115024 (2017).
[70] Y. Kahn, G. Krnjaic, S. Mishra-Sharma, and T. M. P. Tait, Light weakly coupled axial forces: Models, constraints, and projections, J. High Energy Phys. 05 (2017) 002.
[71] C. Bouchiat and P. Fayet, Constraints on the parity-violating couplings of a new gauge boson, Phys. Lett. B **608**, 87 (2005).
[72] H. Davoudiasl, H.-S. Lee, and W. J. Marciano, 'Dark' Z implications for parity violation, rare meson decays, and Higgs physics, Phys. Rev. D **85**, 115019 (2012).
[73] B. Patt and F. Wilczek, Higgs-field portal into hidden sectors, arXiv:hep-ph/0605188.
[74] D. O'Connell, M. J. Ramsey-Musolf, and M. B. Wise, Minimal extension of the standard model scalar Sector, Phys. Rev. D **75**, 037701 (2007).
[75] K. Choi and S. H. Im, Constraints on relaxion windows, J. High Energy Phys. 12 (2016) 093.
[76] G. Belanger, F. Boudjema, A. Pukhov, and A. Semenov, Dark matter direct detection rate in a generic model with micrOMEGAs 2.2, Comput. Phys. Commun. **180**, 747 (2009).
[77] G. Belanger, F. Boudjema, A. Pukhov, and A. Semenov, micrOMEGAs 3: A program for calculating dark matter observables, Comput. Phys. Commun. **185**, 960 (2014).
[78] M. A. Shifman, A. I. Vainshtein, and V. I. Zakharov, Remarks on Higgs boson interactions with nucleons, Phys. Lett. **78B**, 443 (1978).
[79] B. Batell, N. Lange, D. McKeen, M. Pospelov, and A. Ritz, Muon anomalous magnetic moment through the leptonic Higgs portal, Phys. Rev. D **95**, 075003 (2017).
[80] J. Khoury and A. Weltman, Chameleon Fields: Awaiting Surprises for Tests of Gravity in Space, Phys. Rev. Lett. **93**, 171104 (2004).
[81] J. Khoury and A. Weltman, Chameleon cosmology, Phys. Rev. D **69**, 044026 (2004).
[82] P. Brax and C. Burrage, Chameleon-induced atomic afterglow, Phys. Rev. D **82**, 095014 (2010).
[83] P. Brax and C. Burrage, Atomic precision tests and light scalar couplings, Phys. Rev. D **83**, 035020 (2011).
[84] C. Burrage, E. J. Copeland, and E. A. Hinds, Probing dark energy with atom interferometry, J. Cosmol. Astropart. Phys. 03 (2015) 042.
[85] C. Schwob, L. Jozefowski, B. de Beauvoir, L. Hilico, F. Nez, L. Julien, F. Biraben, O. Acef, J. J. Zondy, and A. Clairon, Optical Frequency Measurement of the S-2- D-12 Transitions in Hydrogen and Deuterium: Rydberg Constant and Lamb Shift Determinations, Phys. Rev. Lett. **82**, 4960 (1999).
[86] G. G. Simon, C. Schmitt, F. Borkowski, and V. H. Walther, Absolute electron-proton cross sections at low momentum transfer measured with a high pressure gas target system, Nucl. Phys. **A333**, 381 (1980).
[87] C. Burrage and J. Sakstein, A compendium of chameleon constraints, J. Cosmol. Astropart. Phys. 11 (2016) 045.

[88] A. J. Krasznahorkay *et al.*, Observation of Anomalous Internal Pair Creation in Be8: A Possible Indication of a Light, Neutral Boson, Phys. Rev. Lett. **116**, 042501 (2016).

[89] J. L. Feng, B. Fornal, I. Galon, S. Gardner, J. Smolinsky, T. M. P. Tait, and P. Tanedo, Protophobic Fifth-Force Interpretation of the Observed Anomaly in ^{8}Be Nuclear Transitions, Phys. Rev. Lett. **117**, 071803 (2016).

[90] J. L. Feng, B. Fornal, I. Galon, S. Gardner, J. Smolinsky, T. M. P. Tait, and P. Tanedo, Particle physics models for the 17 MeV anomaly in beryllium nuclear decays, Phys. Rev. D **95**, 035017 (2017).

[91] A. Anastasi *et al.*, Limit on the production of a low-mass vector boson in $e^+e^- \to U\gamma$, $U \to e^+e^-$ with the KLOE experiment, Phys. Lett. B **750**, 633 (2015).

[92] E. M. Riordan *et al.*, A Search for Short Lived Axions in an Electron Beam Dump Experiment, Phys. Rev. Lett. **59**, 755 (1987).